CGI-58 facilitates lipolysis on lipid droplets but is not involved in the vesiculation of lipid droplets caused by hormonal stimulation

Tomohiro Yamaguchi,* Naoto Omatsu,* Emi Morimoto,* Hiromi Nakashima,* Kanki Ueno,* Tamotsu Tanaka,† Kiyoshi Satouchi,† Fumiko Hirose,* and Takashi Osumi[1],*

Graduate School of Life Science,* University of Hyogo, 3-2-1, Koto, Kamigori, Hyogo 678-1297, Japan; and Department of Applied Biological Science,† Fukuyama University, Fukuyama 729-0292, Japan

Abstract A lipid droplet (LD)-associated protein, perilipin, is a critical regulator of lipolysis in adipocytes. We previously showed that Comparative Gene Identification-58 (CGI-58), a product of the causal gene of Chanarin-Dorfman syndrome, interacts with perilipin on LDs. In this study, we investigated the function of CGI-58 using RNA interference. Notably, CGI-58 knockdown caused an abnormal accumulation of LDs in both 3T3-L1 preadipocytes and Hepa1 hepatoma cells. CGI-58 knockdown did not influence the differentiation of 3T3-L1 adipocytes but reduced the activity of both basal and cAMP-dependent protein kinase-stimulated lipolysis. In vitro studies showed that CGI-58 itself does not have lipase/esterase activity, but it enhanced the activity of adipose triglyceride lipase. Upon lipolytic stimulation, endogenous CGI-58 was rapidly dispersed from LDs into the cytosol along with small particulate structures. This shift in localization depends on the phosphorylation of perilipin, because phosphorylated perilipin lost the ability to bind CGI-58. During lipolytic activation, LDs in adipocytes vesiculate into micro-LDs. Using coherent anti-Stokes Raman scattering microscopy, we pursued the formation of micro-LDs in single cells, which seemed to occur in cytoplasmic regions distant from the large central LDs. CGI-58 is not required for this process. Thus, CGI-58 facilitates lipolysis in cooperation with perilipin and other factors, including lipases.—Yamaguchi, T., N. Omatsu, E. Morimoto, H. Nakashima, K. Ueno, T. Tanaka, K. Satouchi, F. Hirose, and T. Osumi. **CGI-58 facilitates lipolysis on lipid droplets but is not involved in the vesiculation of lipid droplets caused by hormonal stimulation.** ***J. Lipid Res.*** **2007.** 48: **1078–1089.**

Supplementary key words Comparative Gene Identification-58 • perilipin • coherent anti-Stokes Raman scattering microscopy

In mammals, excessive energy is stored as triglyceride (TG) in lipid droplets (LDs) of the adipose tissue and supplied to various tissues as fatty acids on demand. Lipolysis in adipocytes, an intimately controlled process whereby TG is hydrolyzed, releasing fatty acids into the circulation, is crucial to the maintenance of the body's energy balance. Stimulation by catecholamines activates the lipolytic response in adipocytes through the increased activity of cAMP-dependent protein kinase (PKA). PKA phosphorylates two key proteins involved in lipolysis: hormone-sensitive lipase (HSL), an enzyme responsible for the hydrolysis of TG and diacylglycerol, and perilipin, a LD-associated protein (1–4). Perilipin blocks the access of HSL to LDs in quiescent adipocytes and thus restricts the lipolytic activity. On the other hand, upon lipolytic activation, multiphosphorylated perilipin facilitates the access of HSL to LDs, thereby promoting lipolysis (5–7). Although HSL has been recognized as the principal rate-limiting factor of TG degradation, recent studies using HSL- and perilipin-null mice revealed that perilipin is a major regulator of lipolysis in adipocytes (8–12). Because perilipin does not have an intrinsic enzyme activity, it seems to serve as a scaffold for the assembly of other proteins in the lipolytic event. Against this background, we previously searched for a binding partner of perilipin and identified Comparative Gene Identification-58 (CGI-58; also called ABHD5) (13). CGI-58, the product of the causal gene of Chanarin-Dorfman syndrome (CDS), interacts with perilipin on the surface of LDs.

CDS is a rare autosomal recessive form of nonbullous congenital ichthyosiform erythroderma, characterized by the abnormal intracellular accumulation of LDs in many tissues (14). We showed that endogenous CGI-58 is distributed predominantly on the surface of LDs in 3T3-L1 cells

Manuscript received 15 November 2006 and in revised form 1 February 2007.

Published, JLR Papers in Press, February 17, 2007.
DOI 10.1194/jlr.M600493-JLR200

Abbreviations: ADRP, adipocyte differentiation-related protein; aP2, adipocyte lipid binding protein; ATGL, adipose triglyceride lipase; CARS, coherent anti-Stokes Raman scattering; CDS, Chanarin-Dorfman syndrome; CGI-58, Comparative Gene Identification-58; GFP, green fluorescent protein; GST, glutathione *S*-transferase; HSL, hormone-sensitive lipase; IBMX, 3-isobutyl-1-methylxanthine; LD, lipid droplet; PKA, cAMP-dependent protein kinase; PPAR, peroxisome proliferator-activated receptor; RNAi, RNA interference; shRNA, short hairpin RNA; TG, triglyceride; TPEF, two-photon excitation fluorescence.

[1] To whom correspondence should be addressed.
e-mail: osumi@sci.u-hyogo.ac.jp

and that its expression is increased during adipocyte differentiation. CGI-58 mutants carrying amino acid substitutions identical to those found in CDS patients were not recruited to LDs, but at the same time they lost the ability to bind to perilipin (13). This observation indicates that the loss of interaction with perilipin is linked to the pathogenesis of CDS. Another research group also demonstrated the interaction of CGI-58 with perilipin (15). They further showed that activation of PKA dispersed CGI-58-green fluorescent protein (GFP) from the surface of LDs to the cytosol, suggesting the involvement of CGI-58 in the lipolytic process. On the other hand, several groups recently showed that adipose triglyceride lipase (ATGL; also called desnutrin or iPLA$_2\zeta$) is an additional TG lipase that catabolizes TG, cooperating with HSL in the adipocytes (16–18). ATGL is expressed in many tissues but at a particularly high level in the adipose tissue. Similar to CGI-58, ATGL is associated with LDs and is believed to be involved in TG turnover on LDs (19). Very recently, CGI-58 was shown to activate ATGL in vitro (20).

To elucidate the regulatory mechanism of lipolysis, it is important to solve the physiological functions of LD proteins involved in this process. In this study, we independently investigated the function of CGI-58 using the RNA interference (RNAi) strategy. We revealed the lipid-catabolizing function of CGI-58 in adipocytes as well as the dynamic behavior of CGI-58 and LDs themselves during lipolytic activation.

EXPERIMENTAL PROCEDURES

Plasmids

cDNA of rat CGI-58 was obtained as described previously (13). cDNAs of rat HSL and mouse ATGL were obtained by RT-PCR from the total RNA of rat adipose tissue and mouse liver, respectively. cDNAs were subcloned into a mammalian expression vector, pCMV5-myc, using appropriate restriction sites. Point mutations of CGI-58 and HSL were generated by PCR and verified by DNA sequencing.

Cell culture

3T3-L1 cells were maintained in DMEM/10% FBS. For differentiation, confluent cells (day 0) were treated with a hormone mixture containing 1 μM dexamethasone, 0.5 mM 3-isobutyl-1-methylxanthine (IBMX), and 5 μg/ml insulin in DMEM/10% FBS. After 48 h (day 2), the hormone mixture was removed and cells were further cultured in DMEM/10% FBS supplemented with 5 μg/ml insulin. The mouse hepatoma cell line Hepa1 was maintained in DMEM/10% FBS. HeLa cells were maintained in F-12/10% FBS. DNA transfection was carried out by the calcium phosphate method (21) for HeLa cells and with Lipofectamine 2000 (Invitrogen) for 293FT cells, according to the manufacturer's directions.

RNAi

Lentivirus expressing short hairpin RNA (shRNA) against mouse CGI-58 was prepared as follows. Pairs of oligonucleotides specifying the shRNA sequences corresponding to the target sequences (AAGAAGTAGTAGACCTAGGTT for CGI-58 RNAi and AAGAAGTAGACATCCTAGGTT for the mismatch control) were designed. A spacer sequence with a loop structure and an extra sequence to facilitate the cloning were also included. The two strands of oligonucleotide were annealed and cloned into pENTER/U6 plasmid (Invitrogen) downstream of the U6 promoter. The cassette containing the U6 promoter and shRNA-coding sequence was then transferred to a self-inactivating lentivirus vector (CS-RfA-EG), generating CS-U6-shRNA-EG. 293FT cells (3.5×10^6) were seeded in 10 cm dishes and cultured for 24 h before transfection. Cells were transfected with a mixture of three plasmids: 7 μg of CSII-U6-shRNA-EG, 5 μg of pCAG-HIVgp, and 4 μg of pCMV-VSV-G-RSV-Rev. The recombinant virus was expected to direct the synthesis of shRNA against CGI-58 under the control of the U6 promoter and GFP under the control of the human elongation factor 1α subunit gene promoter. The culture supernatant containing the recombinant lentivirus was collected 48 h after transfection, passed through a 0.45 μm filter, and used for infection. The titer of lentivirus was estimated by counting the cells expressing GFP after infecting HeLa cells with serially diluted vector stocks. 3T3-L1 preadipocytes or Hepa1 cells were infected with viral stocks at a multiplicity of infection of 50. The transduced cells were grown and used for subsequent experiments.

Antibodies

An antibody was raised in a rabbit against recombinant CGI-58 that was produced by trypsin digestion of glutathione *S*-transferase (GST)-fused CGI-58 expressed in *Escherichia coli*. Guinea pig polyclonal anti-perilipin and anti-adipocyte differentiation-related protein (ADRP) antibodies were purchased from Progen.

RNA analysis

Total RNA was prepared from 3T3-L1 and Hepa1 cells using the RNeasy Mini Kit (Qiagen) according to the manufacturer's instructions. cDNA was synthesized from 1 μg of total RNA in a reaction mixture containing Moloney murine leukemia virus reverse transcriptase (Invitrogen) using a downstream primer mixture (10 pmol each) in a total volume of 20 μl. PCR was performed with 2 μl of the RT product as a template, 10 pmol each of the upstream and downstream primers, and rTaq DNA polymerase (Takara). The reaction products were separated on 2% agarose gels and detected with a fluorescence imaging analyzer (FLA3000; Fuji).

Western blotting

3T3-L1 and Hepa1 cells were washed with PBS and directly dissolved in the heated SDS-PAGE sample buffer. Aliquots of the extracts were subjected to SDS-PAGE and transferred to a nitrocellulose membrane. Proteins were probed with an antibody to CGI-58, perilipin, or ADRP and detected by the ECL method (Amersham Biosciences).

Glycerol release and TG measurements

3T3-L1 cells were grown in 12-well dishes. On day 12 after their differentiation, cells were washed twice with Hank's buffer and incubated with DMEM containing 2% fatty acid-free BSA (Sigma)/20 mM HEPES (pH 7.4) with or without 0.1 mM IBMX at 37°C. After incubation for 3, 6, and 12 h, the medium was collected and assayed for glycerol content using a reagent kit (Wako). Hepa1 cells were treated with a medium containing 0.2 mM oleic acid complexed to albumin for 24 h. Glycerol release was assayed as described above. For TG measurements, Hepa1 cells treated with oleic acid for 48 h were washed and harvested in a lysis buffer (50 mM Tris-HCl, pH 7.4, 150 mM NaCl, 2 mM EDTA, 1% Triton X-100, and 0.5% cholate). Triacylglycerol was measured using a TG E-test kit (Wako).

Fluorescence microscopy

For immunostaining of CGI-58 and perilipin, 3T3-L1 cells were fixed with PBS containing 4% paraformaldehyde, permeabilized in 0.2% Triton X-100/PBS, and blocked with 2% BSA/PBS. Cells were then incubated with primary polyclonal antibodies for 1 h, washed with PBS, and incubated with Cy3-conjugated (Jackson ImmunoResearch) or Alexa488-conjugated (Molecular Probes) secondary antibody for 1 h. After being washed with PBS, cells were mounted and observed with a confocal microscope (LSM510; Carl Zeiss). For detection of GFP-CGI-58 and ADRP, Hepa1 cells were transfected with the expression vector encoding GFP-fused full-length CGI-58. Transfection was carried out using Lipofectamine 2000 (Invitrogen) according to the manufacturer's directions. After transfection for 20 h, cells were fixed, permeabilized with 0.01% digitonin/PBS, and blocked. Cells were immunostained with a primary polyclonal antibody against ADRP and then a Cy3-conjugated secondary antibody. Cells were observed with a fluorescence microscope (Biozero; Keyence). For Nile Red staining, cells were fixed with 4% paraformaldehyde in PBS for 20 min at room temperature and stained with 100 ng/ml Nile Red in PBS for 10 min at room temperature. After being washed with PBS, cells were mounted and observed with a fluorescence microscope.

GST pull-down experiment

Recombinant GST-CGI-58 protein was expressed in *E. coli* BL21(DE3) and affinity-purified with glutathione-agarose. The amount of the recombinant protein was standardized on Coomassie blue-stained SDS-polyacrylamide gels. For the binding experiment with native perilipin and GST-CGI-58, differentiated 3T3-L1 cells (day 8) treated with or without 10 μM isoproterenol and 0.5 mM IBMX for 1 h were washed with Tris-buffered saline (pH 7.4) and harvested in a binding buffer (20 mM Tris-HCl, pH 7.4, 150 mM NaCl, 25 mM 2-glycerophosphate, 50 mM NaF, 1 mM sodium vanadate, 1% Triton X-100, 1 mM EDTA, and 1 mM DTT) containing 1 mM PMSF, a proteinase inhibitor mixture, and a phosphatase inhibitor cocktail (Sigma). The lysates were centrifuged at 15,000 rpm for 15 min at 4°C, and the resulting supernatant was mixed with glutathione-agarose beads containing 15 μg of GST-CGI-58. After 90 min at 4°C, the beads were washed four times with the binding buffer and suspended in 100 μl of the SDS-PAGE loading buffer. The samples (10 μl each) were separated by SDS-PAGE and analyzed by Western blotting with an anti-perilipin polyclonal antibody.

In vitro lipase assay

The transient transfection of HeLa cells by the calcium phosphate method was performed as described (21) using 20 μg of DNA per 10 cm dish. After 24 h, cells overexpressing myc-tagged proteins were harvested and then broken by sonication in 0.25 M sucrose containing 1 mM EDTA, 1 mM DTT, and a proteinase inhibitor mixture. Cell debris was removed by centrifugation, and the supernatant was analyzed for lipase or esterase activity. For the lipase assay, the substrate emulsion was prepared by sonicating the mixture of gum arabic and [^{14}C]triolein. The reaction was performed with 0.2 ml of cell extract and 40 μl of substrate in a buffer (50 mM Tris-HCl, pH 7.4, and 1 mM calcium acetate) for 2 h at 37°C. The reaction was terminated by mixing the solution with 1.5 ml of chloroform and 12 μl of 2.5 N HCl. After centrifugation, the lower layer was collected and dried under a flow of N_2 gas. The lipids were subjected to TLC on a silica gel plate using petroleum ether-diethylether-acetic acid (80:30:1, v/v) as a solvent, and the intensity of the signal for free fatty acid was determined in an imaging analyzer (FLA3000; Fuji). Esterase activity was measured as described previously (22), with minor modifications. Aliquots of cell extracts were incubated in 1 ml of PBS containing 1 mM dithiothreitol and 0.5 mM *p*-nitrophenylbutyrate as a substrate at 37°C for 10 min. The reaction was terminated by adding methanol-chloroform-heptane (10:9:7). The absorbance of the supernatant was measured at 400 nm.

Anti-Stokes Raman scattering microscopy

The construction and operation of a coherent anti-Stokes Raman scattering (CARS) microscope was totally supported by Olympus Co. (Tokyo, Japan). A schematic diagram of the microscope is shown in Fig. 7 below. The system is essentially based on a previously described construction of the forward-detected CARS (F-CARS) microscope (23). There are some modifications. The pulse width is 3–5 ps. The laser beams are directed into a confocal microscope (FV1000/IX81; Olympus). CARS and two-photon excitation fluorescence (TPEF) signals are detected with different types of photomultiplier tube (R3896 for F-CARS and H7422-20 for TPEF; Hamamatsu Photonics).

RESULTS

CGI-58 RNAi causes accumulation of LDs in 3T3-L1 preadipocytes

To investigate the function of CGI-58, we took advantage of the gene-silencing strategy using RNAi. We used a lentivirus-mediated small interfering RNA (siRNA) system in which shRNA corresponding to the target sequence is expressed under the control of the U6 promoter. We initially examined three target sequences in the mRNA of murine CGI-58 for the silencing activity. Among them, the most effective sequence was selected and used throughout the study. As a control, the vector itself or a vector containing a mutant target sequence in which four nucleotides deviated from the wild-type sequence (referred to as a mismatch) was used. 3T3-L1 preadipocytes transduced with each recombinant virus were exposed to the medium containing the adipogenic hormone mixture on the day when the cells reached confluence (day 0) and treated for 2 days. mRNA levels of CGI-58 and markers for adipocyte differentiation [peroxisome proliferator-activated receptor (PPAR)γ and adipocyte lipid binding protein (aP2)] were first examined by RT-PCR (**Fig. 1A**). In control cells, the level of CGI-58 mRNA increased in the course of adipocyte differentiation, similar to a previous finding (13). The level of CGI-58 mRNA was decreased significantly by RNAi compared with the vector or mismatch control, indicating that effective gene silencing was achieved (~80% decrease as quantified by densitometry). On the other hand, mRNA levels of PPARγ and aP2 were not affected by CGI-58 RNAi.

Western blotting also showed that the CGI-58 protein level was decreased significantly in RNAi-treated cells compared with control cells (Fig. 1B). On day 0, a low level of CGI-58 protein was detected in the control cells after prolonged exposure of the membrane, although it is difficult to see in the figure. We also examined protein levels of perilipin and ADRP, the perilipin/ADRP/tail interacting protein of 47 kDa family (PAT) proteins existing on LDs of adipocytes. Although the protein level of perilipin was slightly reduced by CGI-58 RNAi in the early stages of dif-

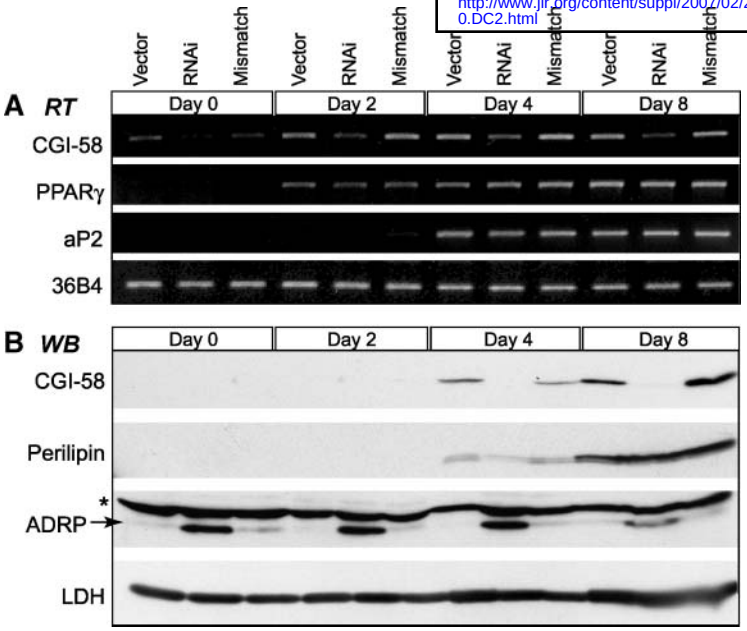

Fig. 1. Comparative Gene Identification-58 (CGI-58) mRNA (A) and protein (B) levels in 3T3-L1 cells subjected to CGI-58 RNA interference (RNAi). A: Total RNA was prepared on the days indicated from 3T3-L1 cells infected with vector, CGI-58 RNAi, or CGI-58 mismatch control lentivirus. The mRNA levels of CGI-58, peroxisome proliferator-activated receptor γ (PPARγ), and adipocyte lipid binding protein (aP2) were measured by RT-PCR (RT). 36B4 was used as an internal control. B: Whole cell lysates were prepared on the days indicated from 3T3-L1 cells treated as described for A and analyzed by Western blotting (WB) with anti-CGI-58, anti-perilipin, and anti-adipocyte differentiation-related protein (ADRP) antibodies. The arrow indicates the band of ADRP, and the asterisk indicates cross-reactive material. Lactose dehydrogenase (LDH) was used as a control.

ferentiation (day 4), almost no difference was observed on day 8 (Fig. 1B). ADRP usually coats the surface of LDs of preadipocytes, whereas it is replaced by perilipin during differentiation into adipocytes. A significant increase in the level of ADRP was observed in the CGI-58 RNAi-treated cells at each stage of differentiation compared with the vector and mismatch controls. On day 8, the amount of ADRP in the CGI-58 RNAi-treated cells was decreased, probably because of disposition from the surface of LDs by perilipin.

Because ADRP is involved in the accumulation of lipids and its protein level closely parallels the total fat cell mass, we examined whether the population and size of LDs are altered in RNAi-treated cells (**Fig. 2**). 3T3-L1 cells treated with CGI-58 RNAi were stained with Nile Red, which labels LDs, and then observed by phase-contrast and fluorescence microscopy. In undifferentiated 3T3-L1 cells, significant differences in the accumulation of LDs were observed between the CGI-58 RNAi and control cells. That is, very few LDs were detectable by Nile Red staining in control preadipocytes, whereas the CGI-58 RNAi preadipocytes exhibited a marked accumulation of LDs (Fig. 2A). Such an abnormal accumulation of LDs was observed in almost all lentivirus-infected cells, which were able to be distinguished by the expression of GFP (data not shown). These results also indicate that CGI-58 protein indeed exists in preadipocytes, albeit at a low level, although it is hardly detectable by Western blotting under normal conditions (Fig. 1B). As shown in Fig. 2B, preadipocytes treated with CGI-58 RNAi differentiated normally and stored large LDs, similar to control cells. In addition, CGI-58 RNAi did not affect the specific activity of glycerol 3-phosphate dehydrogenase, a marker enzyme of adipocytes (data not shown). Together with the unaltered mRNA levels of PPARγ and aP2 in the RNAi cells (Fig. 1A), we conclude that CGI-58 is not necessary for adipocyte differentiation.

CGI-58 RNAi reduced the activity of both basal and PKA-stimulated lipolysis in 3T3-L1 adipocytes

We next examined the lipolytic activity of 3T3-L1 adipocytes treated with CGI-58 small interfering RNA in comparison with that of control cells. Lipolytic activity was estimated by measuring the amount of glycerol released into the medium for both cells in the basal state and cells treated with IBMX to increase the intracellular cAMP level and thus activate PKA (stimulated). **Figure 3** shows the kinetics of glycerol's efflux from the cells. Notably, knockdown of CGI-58 suppressed lipolysis under basal and stimulated conditions compared with the mismatch control. The inhibitory effect of lipolysis by CGI-58 RNAi was more prominent in the stimulated conditions (~50% reduction) than in the basal state (~20%). These results indicate that CGI-58 is involved in lipid turnover on LD surfaces and has a possible function to facilitate lipolysis in 3T3-L1 cells.

CGI-58 contains a canonical esterase/lipase motif, although the active serine residue within the GXSXG motif is replaced by asparagine. Because CGI-58 enhances lipolysis at the cellular level, we next examined whether CGI-58 itself has lipase/esterase activity in vitro (**Fig. 4**). The lipase activity of the extract of HeLa cells expressing rat CGI-58 and its mutant in which asparagine-155 was changed to glycine (N155G) was measured, using a lipid emulsion containing radiolabeled triolein as a substrate. HSL was used as a positive control that has lipase/esterase activity, and HSL S423G (with the active site serine changed to glycine) was used as a negative control. As expected, significant lipase activity was detected in the cell extract containing the wild-type HSL but not in the cell extract containing the S423G mutant (Fig. 4A). On the other hand, CGI-58 and its N155G mutant did not exhibit any lipase activity. Similar results were obtained with respect to esterase activity as monitored with a water-soluble sub-

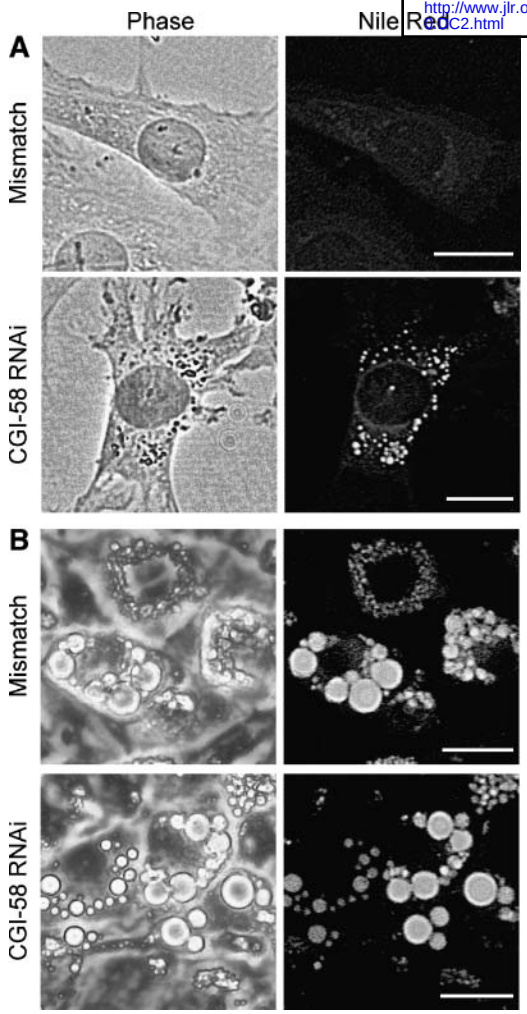

Fig. 2. CGI-58 RNAi causes the accumulation of lipid droplets (LDs) in nondifferentiated 3T3-L1 cells (A) but does not affect adipocyte differentiation (B). 3T3-L1 cells infected with CGI-58 RNAi or mismatch control virus on days 0 (A) and 8 (B) were analyzed by phase-contrast microscopy (left) and Nile Red staining (right) to visualize the LDs. Bars = 20 μm.

strate, *p*-nitrophenylbutyrate (Fig. 4C). HSL and ATGL are representative lipases involved in the degradation of TG in adipocytes. When the cell extract containing HSL or ATGL was combined with an extract containing CGI-58, enhancement of lipase activity was detected compared with the lipase alone, particularly for the combination with ATGL (Fig. 4B). These results suggest that CGI-58 per se does not function as a lipase but has an ability to enhance the activities of TG hydrolases in adipocytes, especially ATGL.

Release of endogenous CGI-58 by lipolytic stimulation from the LD surface is caused by the phosphorylation of perilipin

Lipolytic stimulation by catecholamines causes drastic changes in the protein composition and morphology of LDs in 3T3-L1 cells (24). This stimulation triggers the phosphorylation of perilipin and HSL, followed by the translocation of HSL from the cytosol to the LD surface. Visible fragmentation of LDs then occurs within 1 h, and the micro-LDs generated are dispersed into the cytoplasm (**Fig. 5B**) (6, 25, 26). Perilipin predominantly coats the LDs of mature adipocytes, whereas ADRP does not. After lipolytic stimulation, however, ADRP appears on LDs as a consequence of the increased availability of sites for binding to ADRP on the micro-LDs (24). It was reported that activation of PKA in 3T3-L1 adipocytes disperses exogenously expressed CGI-58-GFP from the surface of LDs to the cytosol (15). Because an overexpressed protein may behave abnormally, we monitored the behavior of endogenous CGI-58 upon lipolytic stimulation by immunofluorescence analysis. Significant dispersion of the protein was visible at as early as 3 min (Fig. 5A), the majority of CGI-58 being redistributed to the cytosol by 5 min, which is considerably faster than the published result for GFP-tagged CGI-58. In contrast, perilipin, a binding partner of CGI-58, was mostly retained on the surface of LDs even 1 h after stimulation (Fig. 5B). Interestingly, we noticed that CGI-58 was also present in particulate structures colocalizing with perilipin in the cells at 1 h after stimulation. The possible significance of these structures is discussed below. Although the phosphorylation of perilipin by PKA was revealed as a shift of electrophoretic mobility by immunoblotting, no significant change was observed in the mobility of CGI-58 (Fig. 5C). The protein level of CGI-58 remained unchanged even 8 h after lipolytic stimulation, indicating that the CGI-58 released from LDs was retained in the cytosol. The time-dependent increase in ADRP possibly correlates with the formation of micro-LDs by lipolytic stimulation (Fig. 5C).

CGI-58 directly interacts with perilipin and is located on LDs in the basal state in 3T3-L1 cells (13, 15). It is also suggested that phosphorylation of serine residues in the C-terminal PKA consensus sites of perilipin A are critical for the translocation of CGI-58 away from the LD surfaces into the cytosol (15). To examine whether the PKA-induced release of CGI-58 from the surface of LDs is attributable to the dissociation of CGI-58 from phosphorylated perilipin, we next performed a GST pull-down assay. GST-fused CGI-58 was mixed with the total cell extracts from nondifferentiated or differentiated 3T3-L1 cells containing unphosphorylated or phosphorylated perilipin, respectively, and recovered with an affinity resin. Figure 5D shows that the unphosphorylated perilipin of the unstimulated cells bound to CGI-58, but the phosphorylated perilipin derived from the stimulated cells was severely impaired in its ability to bind. The observed shift was in fact attributable to the phosphorylation of perilipin, because the band migrated the same as the unphosphorylated perilipin after treatment with alkaline phosphatase (data not shown). Thus, phosphorylated perilipin loses its affinity for CGI-58 and fails to bind CGI-58 on LDs, leading to the release of CGI-58 into the cytosol.

CGI-58 RNAi induces the accumulation of LDs and the expression of ADRP in hepatoma cells

We next examined the effect of CGI-58 RNAi in Hepa1 cells, a cell line derived from mouse hepatoma in which

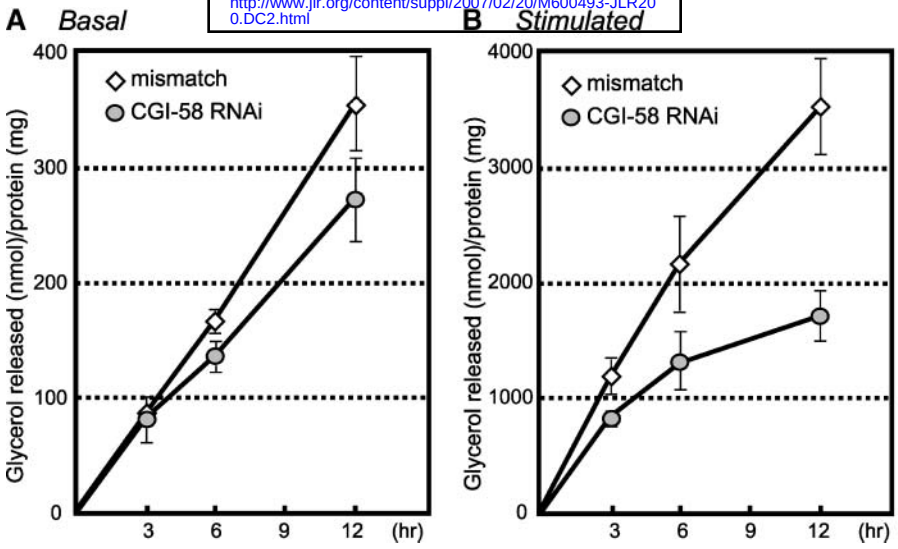

Fig. 3. CGI-58 RNAi reduced both basal and cAMP-dependent protein kinase-stimulated lipolysis in 3T3-L1 adipocytes. Release of glycerol into the medium in the absence (basal) or presence of 3-isobutyl-1-methylxanthine (IBMX; stimulated) was monitored for differentiated 3T3-L1 cells (day 12) infected with CGI-58 RNAi or mismatch control virus. Cells were incubated in DMEM containing 2% fatty acid-free BSA/20 mM HEPES (pH 7.4) with (B) or without (A) 0.1 mM IBMX for up to 12 h at 37°C. Aliquots of medium were collected, and the amount of glycerol released into the medium was measured. Circles and diamonds indicate the efflux of glycerol from CGI-58 RNAi cells and mismatch control cells, respectively. Means of three independent results are given, together with SD.

ADRP but not perilipin is expressed on LDs. Effective gene silencing of CGI-58 was confirmed by RT-PCR (**Fig. 6A**). Many more cycles of PCR were necessary to detect the band of CGI-58 cDNA compared with the 3T3-L1 adipocyte RNA. In addition, the CGI-58 protein band could not be detected by Western blotting, even after prolonged exposure (data not shown). Notably, Hepa1 cells treated with CGI-58 RNAi contained vacuole-like structures in perinuclear regions, in contrast to the control cells, which were confirmed to be enlarged LDs (Fig. 6B, C). It should be emphasized that this accumulation of LDs occurred without the supplementation of fatty acids, which is usually required for LDs to accumulate in nonadipose cells. To assess differences in lipolytic activities, we measured the glycerol release from the CGI-58 RNAi and mismatch control Hepa1 cells. Similar to the result with 3T3-L1 cells, CGI-58 RNAi suppressed the release of glycerol in Hepa1 cells, suggesting a decrease in lipolysis (Fig. 6D, left panel). Consistent with this, cellular TG content was increased in the CGI-58 RNAi cells (Fig. 6D, right panel). The amount of ADRP protein was increased significantly in the RNAi-treated cells accompanied by the formation of LDs (Fig. 6E). When GFP-CGI-58 was expressed in normal Hepa1 cells supplemented with oleic acid, a ring-shaped distribution was observed, colocalizing with ADRP (Fig. 6F). Nile Red staining confirmed this distribution to be on the LD surfaces (data not shown). These results suggest that CGI-58 facilitates lipolysis not only in adipocytes but also in other cell types, consistent with the fact that CDS patients exhibit an abnormal accumulation of LDs in the cells of the whole body, including hepatocytes.

CGI-58 is not involved in the formation of micro-LDs caused by PKA activation

Hormonal stimulation of β-adrenergic receptors triggers a drastic remodeling of LD structures in adipocytes. It is thought that, upon stimulation, the large LDs in mature adipocytes are fragmented into micro-LDs and dispersed throughout the cytosol, although the molecular mechanism of this process is not fully understood (24, 26). We next examined whether CGI-58 is involved in the remodeling of LDs caused by lipolytic stimulation. To do this, we took advantage of a recently established technology, CARS microscopy (**Fig. 7**). This technique creates images of the intracellular distribution of specific molecules using CARS signals. These signals, presented by the equation $2\omega_p - \omega_s$, where ω_p and ω_s denote the frequencies of the pump and Stokes beams, respectively, are maximized by tuning $\omega_p - \omega_s$ to the vibration of specific chemical bonds. Because the C-H bond is most abundant in fatty acids, CARS microscopy is particularly useful for imaging lipids, by capturing the signal of C-H vibration (23). This technique was also shown to be effective for imaging LDs, in which the fatty acyl group is highly accumulated, in live cells without any artificially tagged proteins or fluorescence probes (27). Hence, we expected that, using this technique, we would be able to follow the morphological changes of LDs upon lipolytic activation by time-lapse imaging of a single live cell.

We first observed the process of remodeling of LDs after lipolytic stimulation in differentiated 3T3-L1 cells. As shown in **Fig. 8** and the supplementary video, micro-LDs became visible within 10 min of the addition of isoproterenol and IBMX, and almost all cells carried micro-LDs at

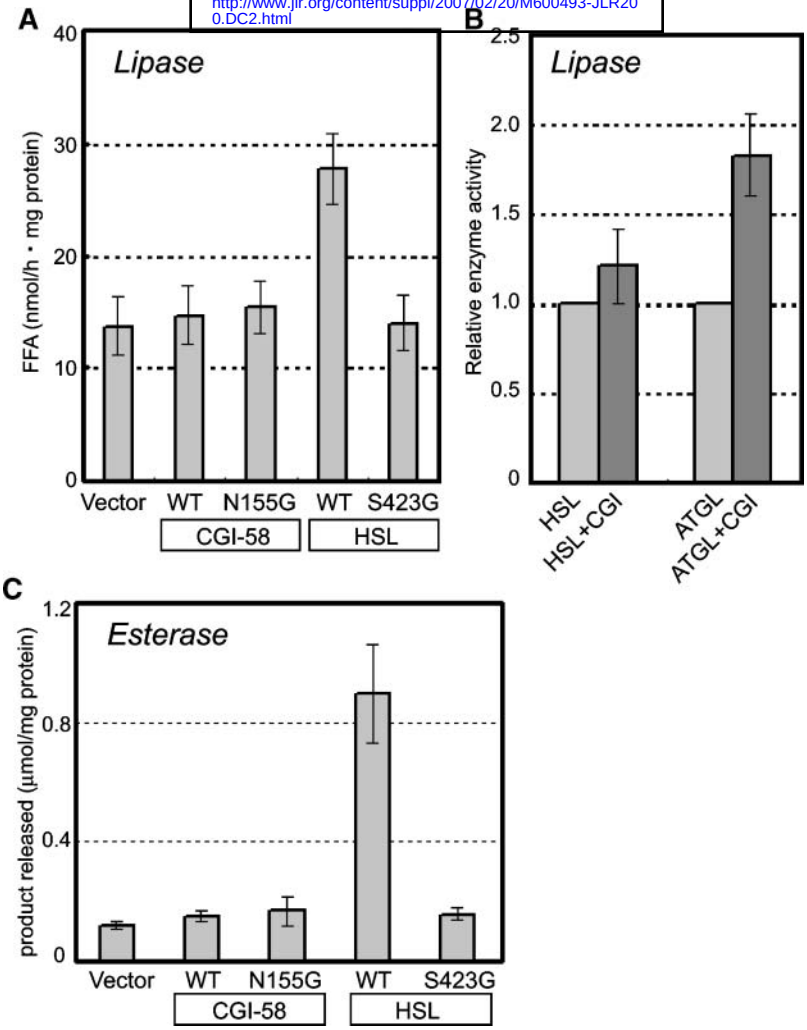

Fig. 4. CGI-58 per se does not act as a lipase but enhances the lipase activity of adipose triglyceride lipase (ATGL). A: HeLa cell homogenates individually expressing myc-tagged CGI-58, hormone-sensitive lipase (HSL), and their derivatives carrying mutations in the putative lipase motifs were analyzed for lipase activities and protein concentrations. The substrate emulsion was prepared by sonicating a mixture of gum arabic and ^{14}C-labeled triolein. The lipids were subjected to TLC, and the radioactivity of free fatty acid was measured in an imaging analyzer. Activity is expressed as nanomoles of free fatty acid released per hour per milligram of protein. B: Homogenates of cells individually expressing HSL and ATGL were mixed with normal cell extracts or extracts containing CGI-58 and analyzed for lipase activity as described for A. Relative enzyme activities are shown. C: Homogenates of cells individually expressing the same proteins as in A were analyzed for esterase activity and total protein. Activity was measured using *p*-nitrophenylbutylate as a substrate and is presented as micromoles of *p*-nitrophenol released per milligram of protein. Means of three independent results are given, together with SD.

no later than 15 min. Because the release of CGI-58 from LDs (Fig. 5A) and translocation of HSL to the surfaces of LDs occurs within 5 min of the stimulation (6), the LDs seem to start remodeling slightly after the mobilization of those proteins. Interestingly, these micro-LDs were not likely to be derived from large central LDs but emerged in distinct positions, such as the perinuclear region or neighboring the plasma membrane. They were oscillating, probably as a result of Brownian motion. The micro-LDs clearly formed gradually during the experiment, reaching diameters of ~1 μm at 60 min after stimulation. Using the same system, we examined the effect of CGI-58 RNAi on the remodeling of LDs in differentiated 3T3-L1 cells. Significant remodeling was observed in the cells treated with CGI-58 RNAi at 60 min after stimulation (**Fig. 9**). Apparently, the fragmentation of LDs was even more marked for the RNAi-treated cells than for control cells, possibly because the RNAi-treated cells at the start of the experiment had smaller and clustered LDs rather than large central LDs. The efficient formation of micro-LDs in the CGI-58 RNAi-treated cells was confirmed in several different cells. Thus, CGI-58 is not required for the vesiculation of LDs during hormone-stimulated lipolysis, although it facilitates the lipolysis on LDs.

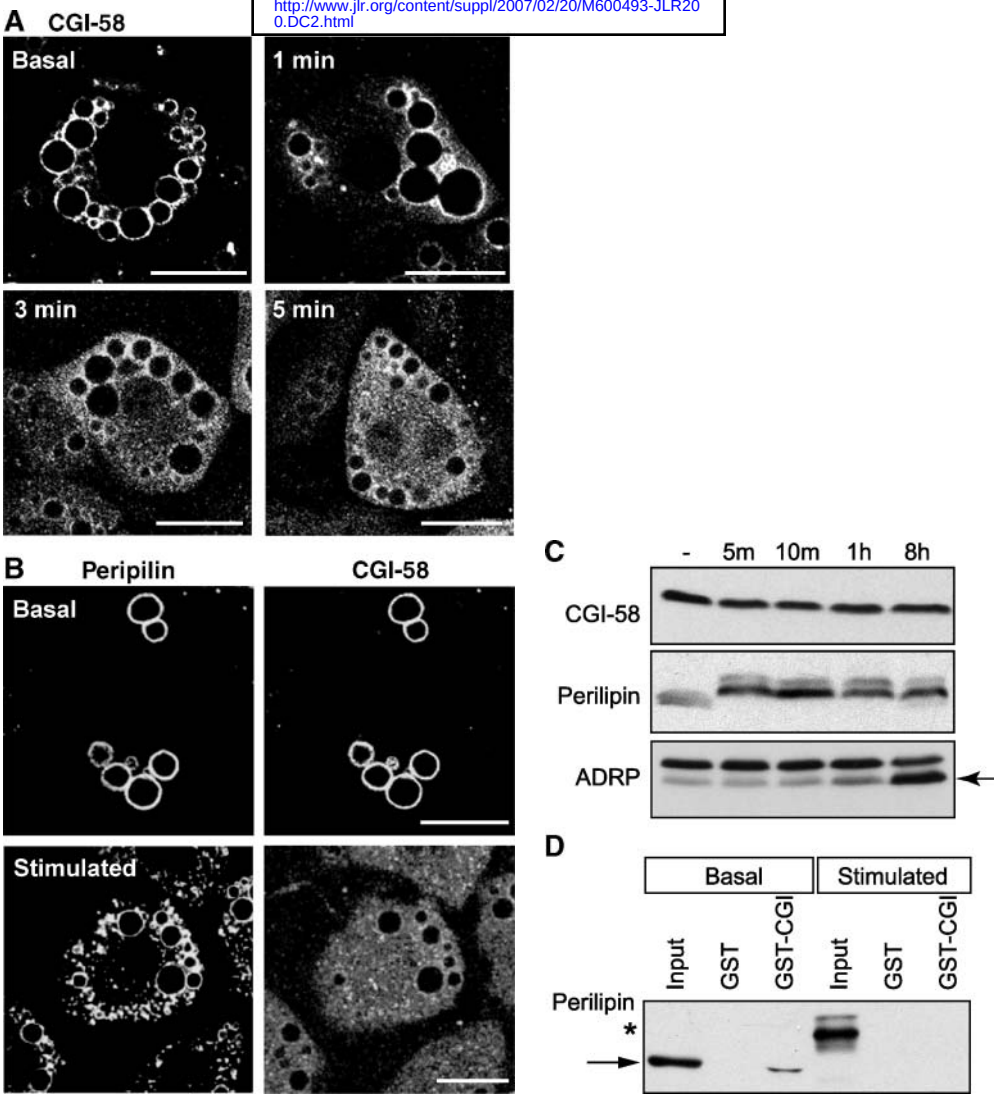

Fig. 5. Endogenous CGI-58 is released from LDs upon lipolytic stimulation depending on the phosphorylation of perilipin. A: Time course of the dissociation of CGI-58 from the surface of LDs. Differentiated 3T3-L1 cells (day 8) were treated with 0.5 mM IBMX and 10 μM isoproterenol and fixed at the indicated time points. CGI-58 was immunostained and observed by confocal microscopy. Bars = 20 μm. B: Differentiated 3T3-L1 cells were fixed and double-immunostained with anti-CGI-58 and anti-perilipin antibodies. The cells were observed with a confocal microscope. The cells were cultured with (stimulated) or without (basal) 0.5 mM IBMX and 10 μM isoproterenol for 1 h before fixation. Bar = 20 μm. C: Differentiated 3T3-L1 cells were lipolytically activated as described above, and cell lysates were prepared at the time points indicated. CGI-58, perilipin, and ADRP proteins in each cell lysate were detected by immunoblotting. The arrow indicates the band of ADRP. D: Direct interaction of glutathione *S*-transferase (GST)-CGI-58 with perilipin is inhibited by phosphorylation of perilipin. 3T3-L1 cells were differentiated (day 8) and incubated with (stimulated) or without (basal) 0.5 mM IBMX and 10 μM isoproterenol for 1 h. The extracts from each of the cells were used as a source of phosphorylated or nonphosphorylated perilipin, and binding with GST-CGI-58 was examined. Input and bound proteins were analyzed by immunoblotting with an anti-perilipin antibody. The arrow indicates the position of nonphosphorylated perilipin A, and the asterisk indicates the phosphorylated form.

DISCUSSION

In this study, we examined the role of CGI-58 on the surface of LDs by applying a loss-of-function strategy using RNAi. Notably, CGI-58 knockdown caused an abnormal accumulation of LDs in both hepatoma cells and preadipocytes. The increase in ADRP in RNAi-treated cells was also consistent with the accumulation of lipids in these cells. CGI-58 RNAi did not affect adipocyte differentiation, as estimated based on glycerol 3-phosphate dehydrogenase activity, or the levels of PPARγ and aP2 mRNA, whereas the RNAi-treated cells exhibited decreased lipolytic activity in both the basal and stimulated states. These results indicate that CGI-58 functions to enhance lipolysis at the cellular

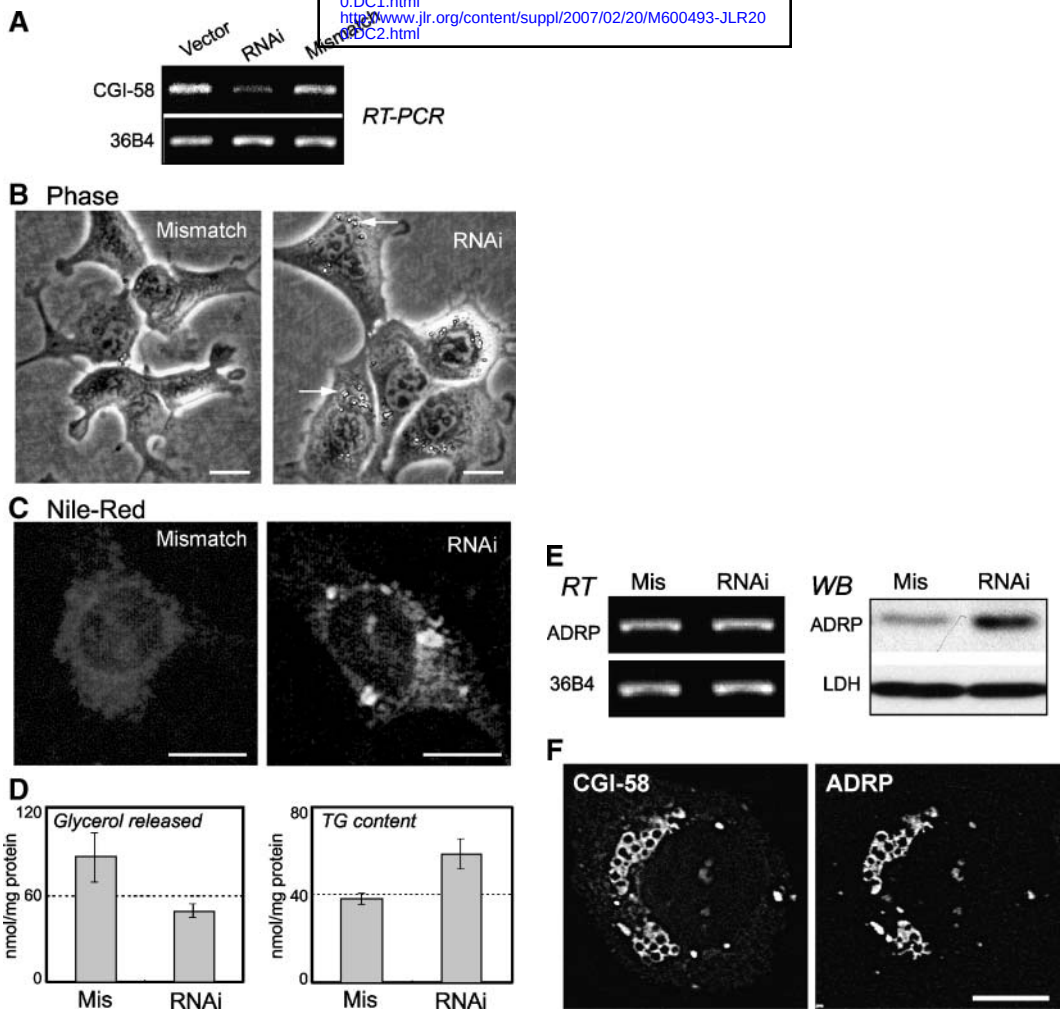

Fig. 6. Effects of CGI-58 RNAi in Hepa1 cells. A: Total RNA was prepared from Hepa1 cells infected with vector, CGI-58 RNAi, or CGI-58 mismatch control virus. The mRNA level of CGI-58 was estimated by RT-PCR. B, C: Hepa1 cells infected with CGI-58 RNAi or mismatch control virus were observed by phase-contrast microscopy (B) and fluorescence microscopy after Nile Red staining (C). A number of enlarged LDs, indicated by arrows, were observed in the CGI-58 RNAi cells in contrast to control cells. Bars = 10 μm. D: Release of glycerol (left) and triglyceride (TG) content (right) were monitored for Hepa1 cells infected with CGI-58 RNAi (RNAi) or mismatch (Mis) control virus. Cells cultured in the presence of 0.2 mM oleic acid were washed and incubated in DMEM containing 2% fatty acid-free BSA for 20 h, and the release of glycerol was determined. For TG measurements, Hepa1 cells treated with oleic acid were washed and harvested in the lysis buffer. The values were normalized by cellular protein contents and given as means ± SD (n = 5). E: Total RNA and whole cell lysates were prepared from Hepa1 cells infected with CGI-58 RNAi and CGI-58 mismatch control virus. The mRNA and protein levels of ADRP were estimated by RT-PCR (RT) and Western blotting (WB), respectively. 36B4 and lactose dehydrogenase (LDH) were used as controls. F: Hepa1 cells expressing green fluorescent protein (GFP)-CGI-58 were fixed and immunolabeled with an antibody to ADRP, followed by Cy3-conjugated secondary antibody. Stained samples were observed by fluorescence microscopy. Bar = 10 μm.

level. On the other hand, it is puzzling why the size or accumulation of LDs is unchanged in the mature adipocytes. In fact, patients with CDS are not typically obese. A possible explanation for this would be that lipid assimilation rather than lipolysis is rate-limiting for the TG accumulation in mature adipocytes in culture as well as in the body. Indeed, even ATGL-null mice were not severely obese, in spite of the critical role of ATGL in lipolysis (28).

Experiments in vitro using the extracts of cells expressing CGI-58 or other proteins showed that CGI-58 per se does not have lipase/esterase activity. Further analysis showed that when CGI-58 was combined with ATGL, lipolytic activity was enhanced significantly compared with the case of ATGL alone. Hence, it is likely that CGI-58 is not a TG hydrolase but acts as a cofactor for a lipase such as ATGL. During the course of this study, the activation of ATGL by CGI-58 in vitro as well as interaction between them was reported (20). Those investigators further showed that mutations of CGI-58 associated with CDS abolished the ability to activate ATGL. Compared with their results, the

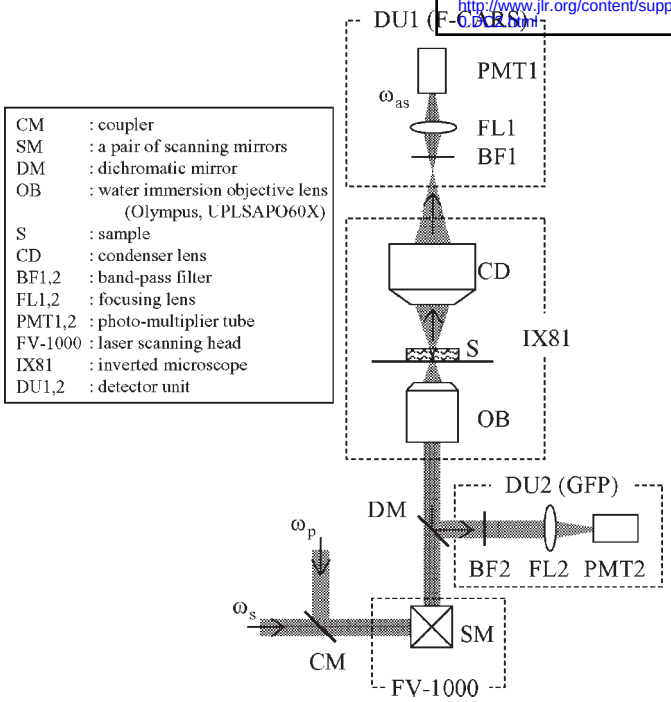

Fig. 7. Scheme of a coherent anti-Stokes Raman scattering (CARS) microscope. A pump beam (ω_p, 712 nm) and a Stokes beam (ω_s, 893 nm) are coaxially combined by a combiner (CM), introduced into an Olympus FV1000/IX81 laser scanning microscope, and focused at the same point in a sample (S) by an objective lens (OB). The forward-detected CARS (F-CARS) beam (ω_{as}, 593 nm) generated in the sample (S) is collected by a condenser lens (CD), goes through the first band-pass filter (BF1) and the first focusing lens (FL1), and then is detected by the first photomultiplier tube (PMT1). At the same time, GFP fluorescence emitted in the sample (S) is collected by the objective lens (OB), reflected aside by a dichromatic mirror (DM), goes through the second band-pass filter (BF2) and the second focusing lens (FL2), and then is detected by the second photomultiplier tube (PMT2).

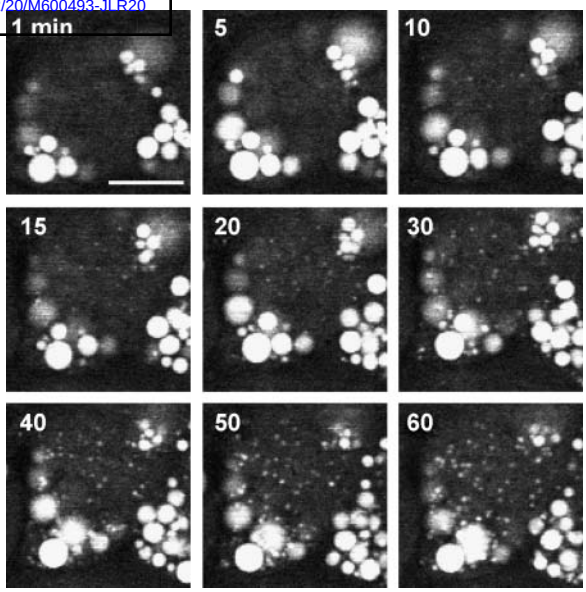

Fig. 8. Time-lapse imaging of the process of LD remodeling by CARS microscopy. Differentiated 3T3-L1 cells (day 8) were treated with 0.5 mM IBMX and 10 μM isoproterenol and imaged in real time by CARS microscopy. Images were taken at 1 min intervals for up to 1 h. Note that micro-LDs appeared at positions distant from the large central LDs (also see the supplementary video). Bar = 10 μm.

activation of ATGL by CGI-58 was less significant in our experiment (20-fold vs. 1.8-fold). Possibly, the sensitivity of our in vitro assay system using gum arabic as a source of micelles was lower than theirs using phospholipid micelles, and hence the effect of CGI-58 was less prominent. On the other hand, we investigated the morphological change in LDs and showed that depletion of CGI-58 by RNAi leads to an increase in the population and size of LDs. This phenotype caused by CGI-58 RNAi is largely similar to that caused by ATGL RNAi reported previously. That is, depletion or overexpression of ATGL in HeLa cells led to an increase or decrease in the size of LDs, respectively (19). These observations suggest that CGI-58 plays an important role in lipid turnover on LDs in concert with ATGL.

It is now accepted that perilipin has a central role in the lipolytic reaction on LDs in adipocytes. Upon activation of the β-adrenergic receptor signaling pathway, perilipin and HSL are phosphorylated by PKA and facilitate lipolysis. CGI-58, recognized as a causal gene of CDS and a binding partner of perilipin in adipocytes in the basal state, has also been suggested to participate in this event (13, 15). CDS is a disorder that involves the abnormal accumulation of lipids in many types of cells throughout the body, and CGI-58 RNAi caused an increase in the formation of LDs and disrupted the release of glycerol at the cellular level. Thus, all of the in vivo and in vitro evidence supports the notion that CGI-58 is indeed a lipolytic factor. On the other hand, CGI-58 translocates from the surface of LDs to the cytosol upon lipolytic stimulation in 3T3-L1 adipocytes, because of its lower affinity for phosphorylated perilipin. Hormonal lipolytic stimulation in mature adipocytes is the

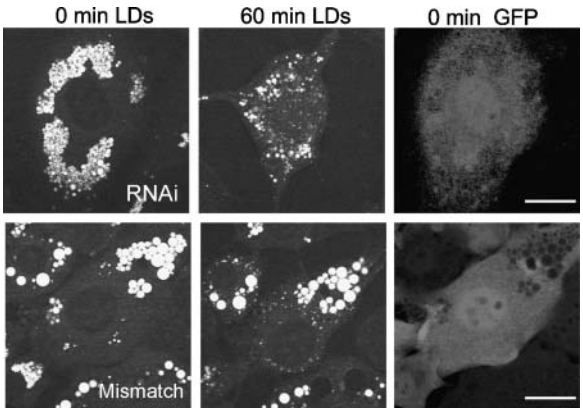

Fig. 9. CGI-58 is not involved in the formation of micro-LDs caused by lipolytic stimulation. 3T3-L1 cells infected with CGI-58 RNAi or mismatch control virus differentiated into adipocytes up to day 8. For both samples, LDs of the same cells were imaged by CARS microscopy before and 1 h after the addition of 0.5 mM IBMX and 10 μM isoproterenol to the medium. Cells were confirmed to be infected by simultaneous imaging of GFP as detected by TPEF. Bars = 20 μm.

most robust TG degradation event in the entire body. Thus, the question arises why CGI-58, a lipolytic factor that is also required for stimulated lipolysis, leaves the LDs during this event. It should be noted that the micro-LDs formed upon lipolytic stimulation seemed to carry both CGI-58 and perilipin on the surface, even after these proteins were released from the central large LDs (Fig. 5). If the micro-LDs are the major sites of active lipolysis, it would be reasonably inferred that CGI-58 has a lipolytic function on their surface. It is also possible that CGI-58 functions not only on the surface of LDs but also in the cytosol. The participation of CGI-58 in lipolysis is also supported by the observation that CGI-58 was retained in the cytosol without being degraded, even after its release from LDs, upon lipolytic stimulation.

Besides the function of CGI-58, we observed an interesting behavior of LDs during lipolysis by CARS microscopy. This technique allows selective real-time imaging of LDs in living cells, without probing with fluorescent dyes or expressing proteins with artificial tags such as GFP. Using this system, we followed the process of the remodeling of LDs caused by lipolytic stimulation. The remodeling process as revealed by time-lapse CARS imaging after lipolytic stimulation was as follows. Initially, micro-LDs appeared within 10 min after stimulation. Although this time varied among cells, almost all cells acquired micro-LDs within 15 min. The amount of time required for LDs to appear in this experiment was much shorter than that observed to date in experiments using fixed cells. Because endogenous CGI-58 starts being released from LDs by 3 min (Fig. 5A) and phosphorylated HSL translocates to LDs by 5 min (6), vesiculation of LDs seems to be a delayed event compared with the mobilization of those proteins. Interestingly, micro-LDs initially arose from all areas of the cytosol, but not from specific regions neighboring the large central LDs. This observation raises the possibility that the micro-LDs are formed from organelles other than the large LDs. Although the mechanism by which LDs form de novo is not fully understood, evidence suggests that the endoplasmic reticulum is a location for the synthesis of LDs (29–31). Thus, the micro-LDs might be formed at the endoplasmic reticulum, responding to the lipolytic stimulation. If this is the case, the micro-LDs are not products of the "fragmentation" of the large central LDs, which has been assumed based on previous observations using fixed cells after prolonged stimulation (24, 26). Assuming that our CARS system can detect LDs as small as ~0.4 μm in diameter as distinct dots, it is possible that extremely small LDs under the limit of detection (referred to here as nano-LDs) emerge from the large central LDs. These nano-LDs are dispersed into the cytosol and then might fuse to each other, consequently becoming the micro-LDs, or they might fuse with the "endoplasmic reticulum-derived" micro-LDs discussed above, thus contributing to their development. Indeed, despite the overall degradation of TG, the micro-LDs grew larger during lipolytic stimulation.

What triggers the vesiculation of LDs? CGI-58 is not essential for this event (Fig. 9), although perilipin likely is (26). Other candidates are Rab family members, which are generally recognized as essential regulators for intracellular membrane trafficking. It is known that Rab18 is recruited to LDs in adipocytes after lipolytic stimulation and increases the amount of endoplasmic reticulum membrane wrapped around LDs (32). Besides Rab18, many other Rab proteins are located on LDs (24, 33, 34), but their functions are not known. CARS microscopy is a powerful tool for studying the dynamic behavior of LDs and, hence, useful for analyzing the molecular mechanisms of LD remodeling.

Based on the present results, we conclude that CGI-58 is a key molecule for lipolysis in almost all cells of the body. Further understanding of the functions of CGI-58 at the molecular level, such as the functional and structural interplay involving CGI-58, PAT proteins, and ATGL, in adipocytes as well as nonadipose cells, should help to elucidate the molecular basis of obesity and its consequence, the metabolic syndrome.

The authors thank S. Hayashi and S. Takimoto (Olympus) for the construction and operation of the CARS microscope. This work was supported in part by grants from the Kao Foundation for Arts and Science (to T.Y.), by Grants-in-Aid for Scientific Research from the Japan Society for the Promotion of Science, and by the 21st Century Center of Excellence Program.

REFERENCES

1. Greenberg, A. S., J. J. Egan, S. A. Wek, N. B. Garty, E. J. Blanchette-Mackie, and C. Londos. 1991. Perilipin, a major hormonally regulated adipocyte-specific phosphoprotein associated with the periphery of lipid storage droplets. *J. Biol. Chem.* **266:** 11341–11346.
2. Fredrikson, G., P. Stralfors, N. O. Nilsson, and P. Belfrage. 1981. Hormone-sensitive lipase of rat adipose tissue. Purification and some properties. *J. Biol. Chem.* **256:** 6311–6320.
3. Holm, C. 2003. Molecular mechanisms regulating hormone-sensitive lipase and lipolysis. *Biochem. Soc. Trans.* **31:** 1120–1124.
4. Tansey, J. T., C. Sztalryd, E. M. Hlavin, A. R. Kimmel, and C. Londos. 2004. The central role of perilipin A in lipid metabolism and adipocyte lipolysis. *IUBMB Life.* **56:** 379–385.
5. Egan, J. J., A. S. Greenberg, M. K. Chang, S. A. Wek, M. C. Moos, Jr., and C. Londos. 1992. Mechanism of hormone-stimulated lipolysis in adipocytes: translocation of hormone-sensitive lipase to the lipid storage droplet. *Proc. Natl. Acad. Sci. USA.* **89:** 8537–8541.
6. Brasaemle, D. L., D. M. Levin, D. C. Adler-Wailes, and C. Londos. 2000. The lipolytic stimulation of 3T3-L1 adipocytes promotes the translocation of hormone-sensitive lipase to the surfaces of lipid storage droplets. *Biochim. Biophys. Acta.* **1483:** 251–262.
7. Sztalryd, C., G. Xu, H. Dorward, J. T. Tansey, J. A. Contreras, A. R. Kimmel, and C. Londos. 2003. Perilipin A is essential for the translocation of hormone-sensitive lipase during lipolytic activation. *J. Cell Biol.* **161:** 1093–1103.
8. Martinez-Botas, J., J. B. Anderson, D. Tessier, A. Lapillonne, B. H. Chang, M. J. Quast, D. Gorenstein, K. H. Chen, and L. Chan. 2000. Absence of perilipin results in leanness and reverses obesity in Lepr(db/db) mice. *Nat. Genet.* **26:** 474–479.
9. Tansey, J. T., C. Sztalryd, J. Gruia-Gray, D. L. Roush, J. V. Zee, O. Gavrilova, M. L. Reitman, C. X. Deng, C. Li, A. R. Kimmel, et al. 2001. Perilipin ablation results in a lean mouse with aberrant adipocyte lipolysis, enhanced leptin production, and resistance to diet-induced obesity. *Proc. Natl. Acad. Sci. USA.* **98:** 6494–6499.
10. Osuga, J., S. Ishibashi, T. Oka, H. Yagyu, R. Tozawa, A. Fujimoto, F. Shionoiri, N. Yahagi, F. B. Kraemer, O. Tsutsumi, et al. 2000. Targeted disruption of hormone-sensitive lipase results in male sterility and adipocyte hypertrophy, but not in obesity. *Proc. Natl. Acad. Sci. USA.* **97:** 787–792.
11. Roduit, R., P. Masiello, S. P. Wang, H. Li, G. A. Mitchell, and M. Prentki. 2001. A role for hormone-sensitive lipase in glucose-

stimulated insulin secretion: a study in hormone sensitive lipase-deficient mice. *Diabetes.* **50:** 1970–1975.
12. Haemmerle, G., R. Zimmermann, M. Hayn, C. Theussl, G. Waeg, E. Wagner, W. Sattler, T. M. Magin, E. F. Wagner, and R. Zechner. 2002. Hormone-sensitive lipase deficiency in mice causes diglyceride accumulation in adipose tissue, muscle, and testis. *J. Biol. Chem.* **277:** 4806–4815.
13. Yamaguchi, T., N. Omatsu, S. Matsushita, and T. Osumi. 2004. CGI-58 interacts with perilipin and is localized to lipid droplets. Possible involvement of CGI-58 mislocalization in Chanarin-Dorfman syndrome. *J. Biol. Chem.* **279:** 30490–30497.
14. Lefèvre, C., F. Jobard, F. Caux, B. Bouadjar, A. Karaduman, R. Heilig, H. Lakhdar, A. Wollenberg, J. L. Verret, J. Weissenbach, et al. 2001. Mutations in CGI-58, the gene encoding a new protein of the esterase/lipase/thioesterase subfamily, in Chanarin-Dorfman syndrome. *Am. J. Hum. Genet.* **69:** 1002–1012.
15. Subramanian, V., A. Rothenberg, C. Gomez, A. W. Cohen, A. Garcia, S. Bhattacharyya, L. Shapiro, G. Dolios, R. Wang, M. P. Lisanti, et al. 2004. Perilipin A mediates the reversible binding of CGI-58 to lipid droplets in 3T3-L1 adipocytes. *J. Biol. Chem.* **279:** 42062–42071.
16. Zimmermann, R., J. G. Strauss, G. Haemmerle, G. Schoiswohl, R. Birner-Gruenberger, M. Riederer, A. Lass, G. Neuberger, F. Eisenhaber, A. Hermetter, et al. 2004. Fat mobilization in adipose tissue is promoted by adipose triglyceride lipase. *Science.* **306:** 1383–1386.
17. Villena, J. A., S. Roy, E. Sarkadi-Nagy, K. H. Kim, and H. S. Sul. 2004. Desnutrin, an adipocyte gene encoding a novel patatin domain-containing protein, is induced by fasting and glucocorticoids: ectopic expression of desnutrin increases triglyceride hydrolysis. *J. Biol. Chem.* **279:** 47066–47075.
18. Jenkins, C. M., D. J. Mancuso, W. Yan, H. F. Sims, B. Gibson, and R. W. Gross. 2004. Identification, cloning, expression, and purification of three novel human calcium-independent phospholipase A2 family members possessing triacylglycerol lipase and acylglycerol transacylase activities. *J. Biol. Chem.* **279:** 48968–48975.
19. Smirnova, E., E. B. Goldberg, K. S. Makarova, L. Lin, W. J. Brown, and C. L. Jackson. 2006. ATGL has a key role in lipid droplet/adiposome degradation in mammalian cells. *EMBO Rep.* **7:** 106–113.
20. Lass, A., R. Zimmermann, G. Haemmerle, M. Riederer, G. Schoiswohl, M. Schweiger, P. Kienesberger, J. G. Strauss, G. Gorkiewicz, and R. Zechner. 2006. Adipose triglyceride lipase-mediated lipolysis of cellular fat stores is activated by CGI-58 and defective in Chanarin-Dorfman syndrome. *Cell Metab.* **3:** 309–319.
21. Sambrook, T., E. F. Fritsch, and T. Maniatis. 1989. Molecular Cloning: A Laboratory Manual, 2nd Ed., Cold Spring Harbor Laboratory Press, Cold Spring Harbor, NY. 16.32–16.36.
22. Holm, C., R. C. Davis, T. Osterlund, M. C. Schotz, and G. Fredrikson. 1994. Identification of the active site serine of hormone-sensitive lipase by site-directed mutagenesis. *FEBS Lett.* **344:** 234–238.
23. Wang, H., Y. Fu, P. Zickmund, R. Shi, and J. X. Cheng. 2005. Coherent anti-Stokes Raman scattering imaging of axonal myelin in live spinal tissues. *Biophys. J.* **89:** 581–591.
24. Brasaemle, D. L., G. Dolios, L. Shapiro, and R. Wang. 2004. Proteomic analysis of proteins associated with lipid droplets of basal and lipolytically stimulated 3T3-L1 adipocytes. *J. Biol. Chem.* **279:** 46835–46842.
25. Londos, C., D. L. Brasaemle, C. J. Schultz, D. C. Adler-Wailes, D. M. Levin, A. R. Kimmel, and C. M. Rondinone. 1999. On the control of lipolysis in adipocytes. *Ann. N. Y. Acad. Sci.* **892:** 155–168.
26. Marcinkiewicz, A., D. Gauthier, A. Garcia, and D. L. Brasaemle. 2006. The phosphorylation of serine 492 of perilipin A directs lipid droplet fragmentation and dispersion. *J. Biol. Chem.* **281:** 11901–11909.
27. Nan, X., J. X. Cheng, and X. S. Xie. 2003. Vibrational imaging of lipid droplets in live fibroblast cells with coherent anti-Stokes Raman scattering microscopy. *J. Lipid Res.* **44:** 2202–2208.
28. Haemmerle, G., A. Lass, R. Zimmermann, G. Gorkiewicz, C. Meyer, J. Rozman, G. Heldmaier, R. Maier, C. Theussl, S. Eder, et al. 2006. Defective lipolysis and altered energy metabolism in mice lacking adipose triglyceride lipase. *Science.* **312:** 734–737.
29. Blanchette-Mackie, E. J., N. K. Dwyer, T. Barber, R. A. Coxey, T. Takeda, C. M. Rondinone, J. L. Theodorakis, A. S. Greenberg, and C. Londos. 1995. Perilipin is located on the surface layer of intracellular lipid droplets in adipocytes. *J. Lipid Res.* **36:** 1211–1226.
30. Murphy, D. J., and J. Vance. 1999. Mechanisms of lipid-body formation. *Trends Biochem. Sci.* **24:** 109–115.
31. Brown, D. A. 2001. Lipid droplets: proteins floating on a pool of fat. *Curr. Biol.* **11:** R446–R449.
32. Martin, S., K. Driessen, S. J. Nixon, M. Zerial, and R. G. Parton. 2005. Regulated localization of Rab18 to lipid droplets: effects of lipolytic stimulation and inhibition of lipid droplet catabolism. *J. Biol. Chem.* **280:** 42325–42335.
33. Liu, P., Y. Ying, Y. Zhao, D. I. Mundy, M. Zhu, and R. G. Anderson. 2004. Chinese hamster ovary K2 cell lipid droplets appear to be metabolic organelles involved in membrane traffic. *J. Biol. Chem.* **279:** 3787–3792.
34. Umlauf, E., E. Csaszar, M. Moertelmaier, G. J. Schuetz, R. G. Parton, and R. Prohaska. 2004. Association of stomatin with lipid bodies. *J. Biol. Chem.* **279:** 23699–23709.